



## Strain Rate Sensitivity Studies of Cryomilled Al Alloy Performed by Nanoindentation

B. Ahn<sup>1, a</sup>, R. Mitra<sup>2, b</sup>, A.M. Hodge<sup>3, c</sup>, E.J. Lavernia<sup>4, d</sup> and S.R. Nutt<sup>1, e</sup>

1. Department of Chemical Engineering and Materials Science, University of Southern California, Los Angeles, CA 90089, USA
2. Department of Metallurgical and Materials Engineering, Indian Institute of Technology, Kharagpur, India
3. Department of Aerospace and Mechanical Engineering, University of Southern California, Los Angeles, CA 90089, USA
4. Department of Chemical Engineering and Materials Science, University of California, Davis, CA 95616, USA

<sup>a</sup>byungahn@usc.edu, <sup>b</sup>rahul@metal.iitkgp.ernet.in, <sup>c</sup>ahodge@usc.edu, <sup>d</sup>lavernia@ucdavis.edu, <sup>e</sup>nutt@usc.edu

**Abstract:** Al 5083 alloy powder was mechanically milled in liquid nitrogen to achieve a nanocrystalline (NC) structure having an average grain size of 50 nm with high thermal stability, and then consolidated by quasi-isostatic (QI) forging. The consolidation resulted in ultrafine grains (UFG) of about 250 nm, and the bulk material exhibited enhanced strength compared to conventionally processed Al 5083. The hardness of as-cryomilled powder and the UFG material was measured by nanoindentation using loading rates in the range of 50–50,000  $\mu\text{N/s}$ , and results were compared with the conventional grain size alloy. Negative strain rate sensitivity was observed in the cryomilled NC powder and the forged UFG plate, while the conventional alloy was relatively strain rate insensitive.

Key words: Cryomilling, nanocrystalline, nanoindentation, hardness, strain rate sensitivity



## 1. Introduction

Nanocrystalline or ultrafine grained materials are often produced by severe plastic deformation (SPD) methods and exhibit significantly enhanced strength and hardness compared to conventional coarse-grained (CG) materials [1, 2]. Cryomilling involves ball milling of metal powders in liquid nitrogen. It has been used to produce bulk nanocrystalline materials with high thermal stability [3–5]. This mechanical attrition process induces repetitive SPD in powders. During cryomilling, the powder particles are heavily deformed by the repeated impact of the balls, leading to a NC structure, which then develops into an UFG structure when the powder has been consolidated. The benefits of milling at cryogenic temperature include accelerated grain refinement, reduced oxygen contamination from the atmosphere, and minimized heat generation. Deformation of bulk NC/UFG materials at various strain rates has been used to investigate mechanisms for improving the strength and ductility of the materials [6–10]. Usually an increase in the flow stress is observed at higher strain rates, indicative of positive strain rate sensitivity (SRS). According to some studies [6–8], the effect of positive SRS becomes significant with decreasing grain size in face-centered cubic (FCC) metals [6–8]. In contrast, body-centered cubic (BCC) metals exhibit decreased SRS with decreasing grain size [7]. However, negative SRS has also been reported for both FCC and BCC metals with NC/UFG structure [9, 10].

Standard bulk specimen testing techniques have been used to evaluate the mechanical properties of materials, including the studies related to determination of SRS. More recent work [9, 10] has relied on characterization of materials at the micro- and nano-scale level. Nanoindentation measurements [11, 12] have been developed to measure mechanical properties locally in small



regions, such as the cross section of powder particles. Such measurements would not be possible using conventional bulk testing methods.

## 2. Experimental procedures

Al 5083 (Al-4.4Mg-0.7Mn-0.15Cr wt.%) gas-atomized powder (by Valimet, Inc., Stockton, CA) was cryomilled in a 20 kg batch with liquid N<sub>2</sub> for 8 hours (DWA Aluminum Composites, Chatsworth, CA). The detailed cryomilling and degassing processes are described elsewhere [13, 14]. For consolidation, the degassed can was pre-heated to 450°C and subsequently QI forged (Advanced Materials & Manufacturing Technologies, LLC). The maximum pressure applied to the die was 343 MPa. The forged disk was machined to remove the canning material, then QI-forged once again. Final dimensions of the disk were 128 mm (diameter) × 16 mm (thickness). A standard Al 5083-H131 ‘armor grade’ plate was used for comparison. The plate was made by conventional processes consisting of casting, followed by hot rolling, and then cold working to the H131 condition.

The concentration of metallic alloying elements was measured using DC plasma emission spectroscopy (by Luvak, Inc.) according to ASTM E1097-03. Non-metallic elements were measured by inert gas fusion methods (RH404 (H), and TCH600 (O & N) analyzers) and by combustion combined with IR detection (CS600 (C) analyzer, LECO, Inc). Samples of the materials, both as-cryomilled powder and forged Al 5083 disk, were prepared for TEM examination (Philips EM420T). Cryomilled powders were prepared by mixing with an epoxy (G-1, Gatan Inc) and curing at ambient temperature, then ground, polished, dimpled and ion milled to perforation for electron transparency. TEM samples from the forged disk were prepared by electrolytic jet polishing using an ethanol



solution containing 8 % perchloric acid + 10 % 2-butoxyethanol at a temperature of - 40°C. Grain size was measured directly from the TEM images using two different methods, a linear intercept method and individual grain measurements for ~ 350 grains generating grain size histograms. In case of the cryomilled powder, the grain size measurements were performed on 6–7 powder particles. The mean grain size and aspect ratio of the standard Al 5083 plate was obtained from optical micrographs after chemical etching using a linear intercept method.

The nanoindentation measurements were performed using a TriboIndenter (Hysitron, Minneapolis, MN) with a 100 nm Berkovich tip. Tests were carried out on resin-mounted Al 5083 alloy samples of the cryomilled NC powder, the forged UFG plate, and the conventional CG alloy. The loading rates were varied between 50 and 50,000  $\mu\text{N/s}$ , and the maximum load used for each test was 5,000  $\mu\text{N}$ . About 25–50 indents were performed at each indentation rate for each specimen. During the tests, the standard nanoindentation drift correction software was applied.

### 3. Results and discussion

Composition of the consolidated cryomilled Al 5083 powder is shown in Table 1, along with the specified composition of standard Al 5083. Examination of the compositions shown in Table 1 indicates that the concentrations of non-metallic elements, N, H, O and C, are much higher in the forged UFG plate made using cryomilled powder than in the specified standard Al 5083 alloy composition. A large fraction of the N, H, O and C are expected to be present as interstitial atoms in the Al 5083 alloy.



**Table 1:** Composition of the forged cryomilled Al 5083, compared with the specification for the standard Al 5083 [14].

Materials	Al [wt. %]	Mg [wt. %]	Mn [wt. %]	Fe [wt. %]	Cr [wt. %]	N [wt. %]	H [ppm]	O [wt. %]	C [wt. %]
Forged UFG plate	92.5	4.46	0.65	0.29	0.07	0.56	27	0.48	0.15
Specification for Al 5083	92.4-95.6	4.0-4.9	0.4-1.0	0.4 max.	0.05-0.25	<0.005 <sup>+</sup>	1.3 <sup>+</sup>	0.003 <sup>+</sup>	0.001 <sup>+</sup>

+ non-metallic elements measured from a standard Al 5083 plate.

The microstructures showing the grain structure of the cryomilled Al 5083 alloy powder and the forged UFG plate, appear in Fig. 1(a) and 1(b), respectively. The selected area diffraction (SAD) patterns from the areas displayed in the bright field TEM images are shown as inserts in Fig. 1(a) and 1(b). The SAD pattern shown in Fig. 1(a) from as-cryomilled NC powder shows only rings, which are characteristic of randomly distributed nano-size grains. On the other hand, individual spots arranged in rings are distinguishable in the SAD pattern shown in Fig. 1(b) from the consolidated UFG material. The spots in the SAD pattern arise from the CG structure. Histograms depicting the grain size distributions in the cryomilled powder and in the forged UFG plate are also shown in Fig. 2(a) and 2(b), respectively. The average grain size of all three materials along with the aspect ratio of the grains, the cryomilled NC powder, the forged UFG plate and the standard CG plate, is shown in Table 2. The average grain size in the cryomilled NC powder (50 nm) is less than a fifth of that (254 nm) in the forged UFG plate. In addition, the grain size distribution of the forged UFG material is much wider than that of the NC powder, and the sizes of the conventional CG material are an order of magnitude larger. The larger average grain size and the wider grain size distribution in the forged UFG material (compared to the cryomilled NC powders) is attributed to grain coarsening during consolidation at high temperature. The average grain size for the conventional CG material is three orders of magnitude greater than that in the forged UFG material, as shown in Table 2.

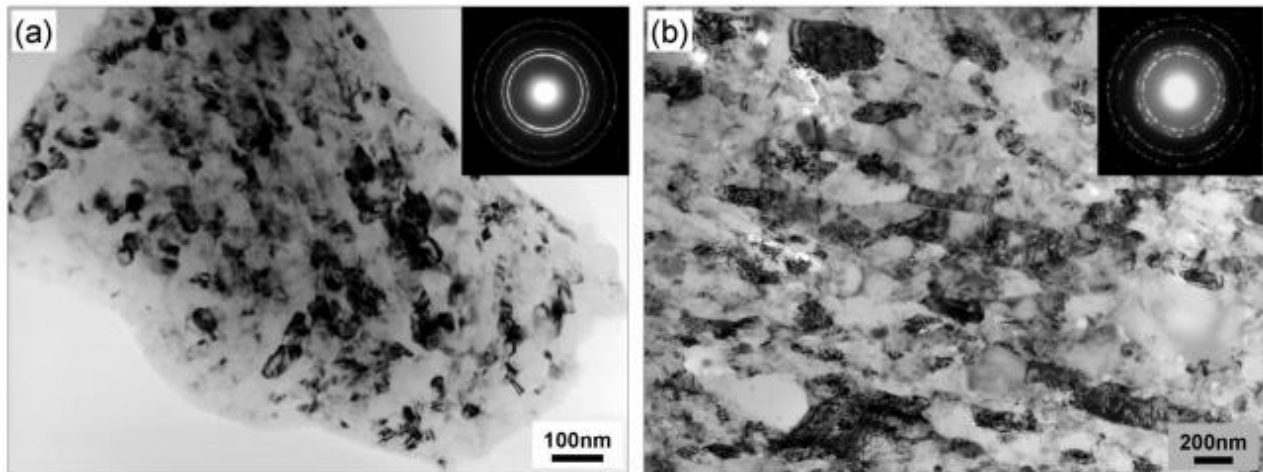


**Figure 1:** TEM bright field micrographs of (a) as-cryomilled NC powder and (b) forged UFG plate with corresponding SAD patterns.

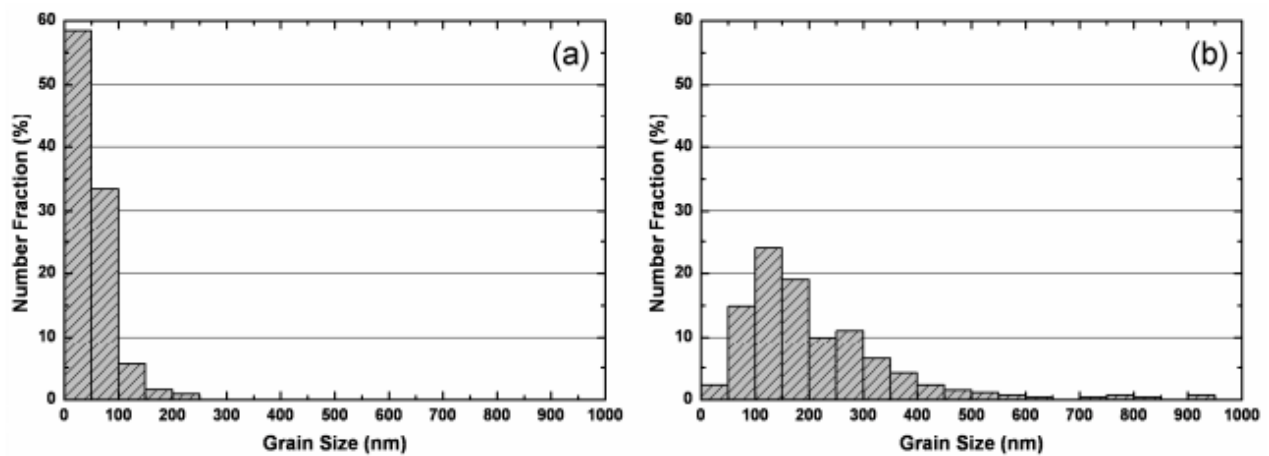


**Figure 2:** Histograms of the grain size distribution of (a) as-cryomilled NC powder and (b) forged UFG plate viewed normal to the forging direction.

**Table 2:** Mean grain size and aspect ratio of as-cryomilled NC powder, the forged UFG plate, and the standard Al 5083 plate (measured from TEM micrographs and optical micrographs).

Materials	Individual Grains		Linear Intercept Method	
	Average Size	Aspect Ratio	Average Size	Aspect Ratio
As-cryomilled NC powder	50 nm	1.5	-	-
Forged UFG plate*	252 nm	1.8	254 nm	1.7
Standard Al 5083 plate <sup>+</sup>	-	-	132 $\mu$ m	6.5

\*viewed normal to the forging direction; + viewed normal to the rolling direction.



Data showing the variation of hardness with loading rate for the cryomilled NC powder, the forged UFG material, and the conventional CG material are shown in Table 3. The standard deviations are shown as error bars for each test result. From a careful study of the data, the following may be inferred: (i) the standard deviations of the hardness values are greater for the cryomilled NC powder and the forged UFG material than for the conventional CG material; (ii) the hardness decreases with increasing loading rate for the NC powder and the UFG material, while it remains unchanged for the CG material; (iii) the drop in hardness with loading rate for the NC powder is much sharper than for the UFG material; (iv) the average hardness of the UFG material is 2.5–3 times greater than the CG alloy, depending on the loading rate; and (v) the hardness of the NC powder is 8 and 6 times greater than the CG material at the highest and the lowest loading rates, respectively. The greater standard deviations for hardness values obtained from the cryomilled powder and the forged UFG sample are attributed to microstructural heterogeneities, particularly due to the width of the grain size distributions, as depicted in Fig. 2(a) and 2(b). On the other hand, the conventional alloy has much less scatter in grain size. The higher hardness values in samples with finer grain sizes (50 nm) follows expectations based on the Hall-Petch relationship. The decrease in the hardness with loading rate indicates negative strain rate sensitivity in these alloys, particularly when the average grain size is less than 100 nm.

The negative SRS observed during the nanoindentation experiments is usually observed in materials exhibiting dynamic strain aging during tension tests [15]. Room temperature tensile experiments on these alloys have shown evidence of serrated plastic flow behavior [16], which has been attributed to dynamic strain aging. The dynamic strain aging is caused by the attractive interaction of dislocations with interstitial solute atoms. Interstitial solute atoms of nitrogen, carbon,



hydrogen and oxygen pin the dislocation cores and exert drag on dislocation glide. The pinning of dislocations by the interstitial solute atoms causes jerky glide of the dislocations. At high loading rates or strain rates, there is a rapid increase in the density of mobile dislocations, particularly when the dislocations are locked-in and are not free to move otherwise. The larger plastic deformation accompanying the generation of increased density of mobile dislocations manifests as larger indentation size and lower hardness. Both the density of dislocations and their mobility decreases as the grain size decreases, and this is particularly pronounced when the average grain size is less than 100 nm. Hence, the effect of higher loading rates on triggering of dislocation motion is more pronounced when the grain size is in the nanocrystalline range.

Negative SRS has also been observed in NC BCC metals, and has been attributed to twinning [10]. Evidence of deformation twinning during cryomilling has also been reported for FCC metals [17]. Furthermore, Jin et al. [18] have reported grain growth during room temperature nanoindentation of UFG high purity Al. Grain growth could result at high loading rates and could lead to softening. However, TEM studies of the NC Al 5083 alloy powders subjected to a series of hardness indentations have shown no evidence of deformation twinning or grain growth. Grain growth is inhibited at room temperature because of the presence of solutes and interstitial impurity 224 Nanomaterials by Severe Plastic Deformation IV atoms, as well as by-products of cryomilling, including oxides and nitrides [4]. Hence, the role of interstitial solute atoms in pinning the dislocations provides the most plausible explanation for negative SRS observed during nanoindentation of the cryomilled NC powders at different loading rates.



**Table 3:** Hardness variations of the cryomilled NC powder, the forged UFG plate and the standard Al 5083-H131 plate with respect to loading rates.

Materials	Hardness [GPa] for Loading Rates		
	50 $\mu\text{N/s}$	1,000 $\mu\text{N/s}$	50,000 $\mu\text{N/s}$
As-cryomilled NC powder	$4.1 \pm 0.3$	$3.4 \pm 0.3$	$3.1 \pm 0.3$
Forged UFG plate	$2.6 \pm 0.2$	$2.3 \pm 0.2$	$2.3 \pm 0.2$
Standard Al 5083 plate	$1.6 \pm 0.1$	$1.6 \pm 0.1$	$1.6 \pm 0.1$

## 4. Conclusions

The effect of loading rate on the hardness obtained from nanoindentation experiments on Al 5083 alloy in the form of cryomilled NC powders, forged UFG as well as conventional CG materials with the average grain size of 50 nm, 253 nm and 132  $\mu\text{m}$ , respectively, has been examined. For a specific loading rate, the hardness increases with decreasing grain size, as expected from the Hall-Petch relationship. The hardness decreases sharply with loading rate in the cryomilled NC powder, indicating significant negative SRS. The negative SRS is less prominent in the UFG material and absent in the conventional CG alloy. The negative SRS in the NC and UFG materials is attributed to the pinning of dislocations by interstitial solute atoms as well as the small grain size, both of which restrict dislocation motion. Indentation at high loading rates is expected to trigger dislocation motion by unlocking from solute atoms, increasing the density of mobile dislocations. This will result in an increase in the size of the indentation, and a reduction in hardness.



**Acknowledgements:** Financial support was provided by the Office of Naval Research under contract N00014-03-C- 0163. The authors gratefully acknowledge Troy D. Topping of UC Davis and A. Piers Newbery previously of UC Davis for their assistance.

## References:

1. H. Gleiter: *Prog. Mater. Sci.* Vol. 33 (1989), p. 223
2. C. Suryanarayana: *Int. Mater. Rev.* Vol. 40 (1995), p. 41
3. F. Zhou, J. Lee, S. Dallek, and E.J. Lavernia: *J. Mater. Res.* Vol. 16(12) (2001), p. 3451
4. D.B. Witkin and E.J. Lavernia: *Prog. Mater. Sci.* Vol. 51 (2006), p. 1
5. A.P. Newbery, B.Q. Han, E.J. Lavernia, C. Suryanarayana and J.A. Christodoulou in: *Materials Processing Handbook*, edited by J.R. Groza, J.F. Shackelford, E.J. Lavernia and M.T. Powers, CRC Press, Boca Raton, FA (2007), pp. 13-1–13-28.
6. R. Schwaiger, B. Moser, M. Dao, N. Chollacoop and S. Suresh: *Acta Mater.* Vol. 51 (2003), p. 5159
7. Q. Wei, S. Cheng, K.T. Ramesh and E. Ma: *Mater. Sci. Eng. A* Vol. 381 (2004), p. 71 *Materials Science Forum* Vols. 584-586 225
8. B.Q. Han, J.Y. Huang, Y.T. Zhu and E.J. Lavernia: *Scripta Mater.* Vol. 54 (2006), p. 1175
9. B.Q. Han, J. Huang, Y.T. Zhu and E.J. Lavernia: *Adv. Eng. Mater.* Vol. 8(10) (2006), p. 945
10. Y.M. Wang, A.M. Hodge, P.M. Bythrow, T.W. Barbee, Jr. and A.V. Hamza: *Appl. Phys. Lett.* Vol. 89 (2006), 081903
11. W.C. Oliver and G.M. Pharr: *J. Mater. Res.* Vol. 7 (1992), p. 1564
12. G.M. Pharr, W.C. Oliver and F.R. Brotzen: *J. Mater. Res.* Vol. 7 (1992), p. 613
13. B. Ahn, A.P. Newbery, E.J. Lavernia and S.R. Nutt: *Mater. Sci. Eng. A* Vol. 463 (2007), p. 61
14. A.P. Newbery, B. Ahn, R.W. Hayes, P.S. Pao, S.R. Nutt and E.J. Lavernia: *Metall. Mater. Trans. A* (2008), in press.
15. P. Rodriguez: *Bull. Mater. Sci.*, Vol. 6 (1984), p. 653
16. D. Witkin, B.Q. Han and E.J. Lavernia: *Metall. Mater. Trans. A*, Vol. 37A (2006), p. 185
17. Y.T. Zhu, X.Z. Liao, S.G. Srinivasan, Y.H. Zhao, M.I. Baskes, F. Zhou, E.J. Lavernia: *Appl. Phys. Lett.* Vol. 85 (2004), p.5049
18. M. Jin, A.M. Minor, E.A. Stach and J.W. Morris, Jr.: *Acta Mater.* Vol. 52 (2004), p. 5381